Electronic Supplementary Information

Rigidochromism of Tetranuclear Cu(I)–Pyrazolate Macrocycles: Steric Crowding with Trifluoromethyl Groups

Shinaj K. Ragajopal,[1] Matthias Zeller,[1] Sergei Savikhin,[2] Lyudmila V. Slipchenko,[1] and Alexander Wei[1,3,*]

[1] James and Margaret Tarpo Department of Chemistry, 560 Oval Drive, Purdue University, West Lafayette, IN 47907, USA

[2] Department of Physics and Astronomy, 525 Northwestern Avenue, Purdue University, West Lafayette, IN 47907, USA

[3] School of Materials Engineering, Purdue University, 701 W. Stadium Avenue, West Lafayette, IN 47907, USA

Table of Contents

1. General information and materials and methods

Chemical reagents and supplies obtained from commercial vendors were used as received unless otherwise noted. ^1H, ^{13}C and ^{19}F NMR spectra were collected at room temperature on a Varian INOVA 300 or Bruker NEO500 spectrometer. NMR samples were prepared in chloroform-d with chemical shifts (δ) reported in ppm relative to residual non-deuterated solvent resonances as internal standards. Elemental analysis of Cu_4pz_4 complex **4** was performed on dry powder using an atmospheric solid analysis probe. Full details on the synthesis and characterization of Cu_4pz_4 complex **4** and their intermediates are described in the respective sections below.

Single-crystal samples for x-ray diffraction were grown in CH_2Cl_2–toluene mixtures with slow evaporation at rt. Thin-film samples were prepared on quartz substrates cleaned ultrasonically with toluene, acetone and 2-propanol, followed by plasma treatment for 10 min using a Harrick plasma cleaner PDC-XG3. Cu_4pz_4 complexes in dichloromethane (5 mg/mL) were filtered through a 0.2-μm PTFE membrane (Whatman), cast onto quartz substrates using a SPS Polos SPIN 150i spin coater (5000 rpm, 30 s), then dried at rt for 30 min under vacuum (Fisher Scientific Isotemp® Vacuum Oven, Model 281A).

Absorption spectra were acquired on a Varian Cary50 Bio UV-visible spectrophotometer using a 1-cm quartz cuvette. Photoluminescence (PL) spectra and absolute quantum yields (Φ_{PL}) were measured using an Edinburgh Instruments FLS 980 spectrometer with an integrating sphere accessory. PL lifetimes (τ) and variable-temperature analyses were measured using a Varian Cary Eclipse spectrophotometer using a quartz tube (5 mm outer diameter, 4 mm inner diameter, 77 mm tube length, Wilmad-LabGlass) or a quartz substrate using an excitation wavelength of 270 nm; τ values of solid-state samples were obtained from mono-exponential fits to the data at room temperature (297 K).

Quantum chemical calculations were performed using a hybrid density functional theory (DFT) functional (Gaussian 16).[S1] Angle constraints and relaxed potential energy surface scans of pyrazole ligands were performed at the PBE1PBE/LanL2DZ level using the ModRedundant keyword in Gaussian 16. Geometries of Cu_4pz_4 complexes were optimized from crystal structures at the PBE0/TZVP level with the LANL2DZ basis set used with an effective core potential (ECP) addition to Cu atoms for the ground state in the gas phase. Time-dependent DFT (TD-DFT) was performed at the PBE0/TZVP with a LANL2DZ basis set for the ECP addition to Cu atoms in the gas phase.

2. Synthesis

3,5-Di-*tert*-butyl-4-iodo-1*H*-pyrazole (3,5-di-^{t}Bu$_2$-4-I-pz)[S2]

3,5-^{t}Bu$_2$-4-I-pz
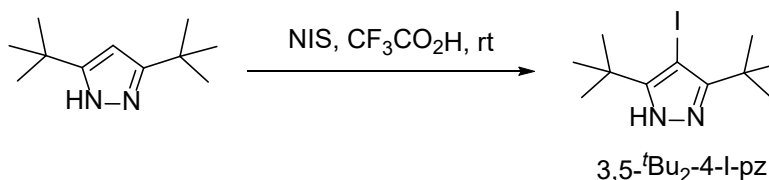
This compound was prepared using previously reported conditions for a similar derivative.[1] 3,5-di-*tert*-butyl-1*H*-pyrazole (100 mg, 0.6 mmol) was dissolved in 1.0 mL of TFA. *N*-iodosuccinimide (124.8 mg, 0.6 mmol) was added in one portion and the reaction was stirred at rt for 1 h. Water and EtOAc were added, and the phases were separated. The organic phase was washed with saturated aqueous sodium sulfite and dried over sodium sulfate, then filtered and concentrated. The crude product was passed through a silica gel plug and concentrated to yield 4-iodopyrazole as a pure white solid (160 mg, 94%). ^{1}H NMR (500 MHz, CDCl$_3$) δ 10.97 (1H, bs), 1.0 (18H, s). ^{13}C NMR (126 MHz, CDCl$_3$) δ 159.54, 52.85, 32.98, 29.12.

1-Benzyl-3,5-di-*tert*-butyl-4-iodo-pyrazole (1-Bn-3,5-di-^{t}Bu$_2$-4-I-pz)[S3]

3,5-di-^{t}Bu$_2$-4-I-pz   1-Bn-3,5-^{t}Bu$_2$-4-I-pz
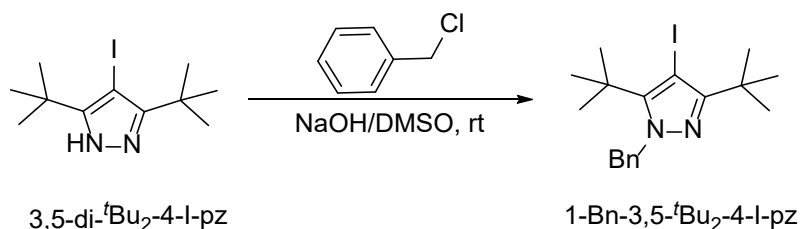
3,5-di-^{t}Bu$_2$-4-I-pz (1.0 g, 3.3 mmol) and benzyl chloride (3.6 mL, 29.9 mmol) were dissolved in 20 mL of anhydrous DMSO (5 mL) and treated with 1.6 equiv of powdered NaOH (0.21 g, 5.3 mmol), resulting in a warm solution. The reaction mixture was cooled to rt and stirred for 12 h, then treated with water (50 mL), extracted with ethyl acetate (100 mL), and washed with aq. NaHCO$_3$ (2 × 75 mL). The organic extract was dried over Na$_2$SO$_4$, filtered and concentrated, then purified by gradient silica gel chromatography (30% DCM:Hexane) to yield **1-Bn-3,5-di-^{t}Bu$_2$-4-I-pz** as white solid (1.20 g, 92.7% yield). ^{1}H NMR (500 MHz, CDCl$_3$) δ 7.30-7.28 (2H, m), 7.29 (1H, m), 6.79-6.77 (2H, m), 5.61 (2H, s), 1.49 (9H, s), 1.45 (9H, s). ^{13}C NMR (126 MHz, CDCl$_3$) δ 158.09, 148.62, 139.46, 128.64, 127.12, 125.46, 57.69, 56.16, 33.98, 33.67, 30.90, 29.46.

1-Benzyl-3,5-di-*tert*-butyl-4-trifluoromethyl-1*H*-pyrazole (1-Bn-3,5-di-*^{t}*Bu$_2$-4-CF$_3$-pz)[S4]

1-Bn-3,5-*^{t}*Bu$_2$-4-I-pz   1-Bn-3,5-*^{t}*Bu$_2$-4-(CF$_3$)-pz
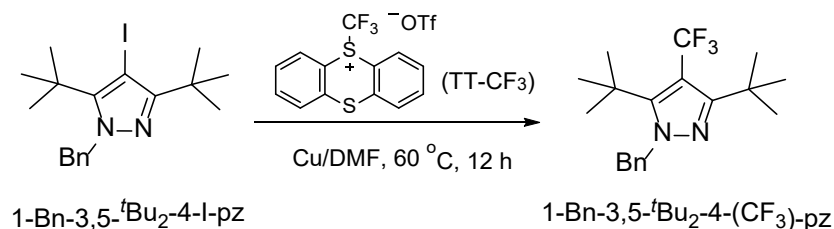
S-Trifluoromethylthianthrenium triflate (TT-CF$_3$) was prepared using the method described of Ritter and co-workers.[2] A 100-mL, two-neck, round-bottomed flask equipped with a teflon-coated magnetic stirring bar was charged with thianthrene (3 g; 1.38 mmol) and CH$_2$Cl$_2$ (36 mL; 0.4 M). 1.1 equiv of triflic anhydride (2.6 mL, 1.52 mmol) was added in one portion at room temperature, which rapidly turned the reaction mixture light purple with gradual darkening, accompanied by the formation of suspended particles. The reaction mixture was stirred at 35 °C for 22 h, then treated carefully with saturated aq NaHCO$_3$ (17.5 mL) which turned the suspension light brown. The biphasic mixture was separated, and the organic layer was concentrated to dryness to a light brown residue. Diethyl ether was added, and the yellowish suspension was stirred vigorously at rt for 30 min followed by careful decanting of the supernatant, and repeated up to four times. The final slurry was concentrated to dryness to yield crude TT-CF$_3$ as a pale-yellow solid, which was purified further by recrystallization from a CH$_2$Cl$_2$–pentane mixture to afford a colorless solid (3.6 g, 60%).

1-Bn-3,5-di-*^{t}*Bu$_2$-4-I-pz (100 mg, 0.25 mmol) and 2 equiv TT-CF$_3$ (219.5 mg, 0.5 mmol) were dissolved in anhydrous DMF (1 mL) and treated with activated Cu powder (43.3 mg, 0.76 mmol). The mixture was then stirred at 60°C under argon for 12 hours or until the TLC indicated full disappearance of starting material, then cooled to rt. The reaction mixture was diluted with ethyl acetate (30 mL), washed with H$_2$O (3 × 10 mL), dried over Na$_2$SO$_4$ and concentrated, then purified by silica gel chromatography using 3:1 petroleum ether:CH$_2$Cl$_2$ to yield **1-Bn-3,5-di-*^{t}*Bu$_2$-4-CF$_3$-pz** as a white solid (75 mg, 88%). ^{1}H NMR: δ 7.32-7.29 (m, 2H), 7.24 (m, 1H), 6.90 (d, *J* 7.3 Hz, 2H), 5.57 (s, 2H), 1.38 (s, 9H), 1.34 (s, 9H). ^{19}F NMR (101 MHz, CDCl$_3$): –45.12 (s). ^{13}C NMR (126 MHz, CDCl$_3$): δ 157.34, 151.40, 138.15, 128.53, 127.23, 125.85, 127.08–123.15 (q, *J* 127.2 Hz), 107.88–107.0 (q, *J* 37.0 Hz), 56.91, 33.91, 33.68, 31.02, 30.21.

3,5-di-*tert*-butyl-4-(trifluoromethyl)-1*H*-pyrazole (3,5-^{t}Bu$_2$-4-CF$_3$-pz; 4)[S5]

1-Bn-3,5-^{t}Bu$_2$-4-CF$_3$-pz   3,5-^{t}Bu$_2$-4-CF$_3$-pz (**4**)
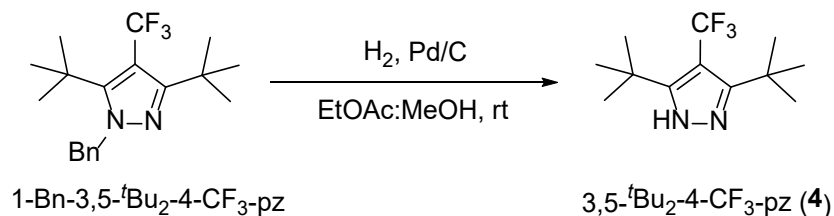
1-Bn-3,5-di-^{t}Bu$_2$-4-CF$_3$-pz (50 mg, 0.64 mmol) was dissolved in 1:1 methanol:ethyl acetate (2 mL) and treated with 5% palladium on charcoal (32 mg, 0.01 mmol). The mixture was charged several times with H$_2$ then stirred for 1 hour at rt and 1 atm. The reaction mixture was filtered over Celite, concentrated and passed through a silica gel plug (30% EtOAc:Hexane) to afford pyrazole **4** as a white solid (35.7 mg, 97%). ^{1}H NMR (500 MHz, CDCl$_3$) δ 10.97 (1H, bs), 1.39 (18H, s). ^{19}F NMR (101 MHz, CDCl$_3$): δ –47.33 (s). ^{13}C NMR (126 MHz, CDCl$_3$) δ 156.24, 127.46–121.11 (q, *J* 266.4 Hz), 105.99–105.09 (q, *J* 37.6 Hz), 33.23, 29.84.

Cu$_4$(3,5-^{t}Bu$_2$-4-CF$_3$-pz)$_4$ complex (3)[S6]

3,5-^{t}Bu$_2$-4-CF$_3$-pz (**4**)
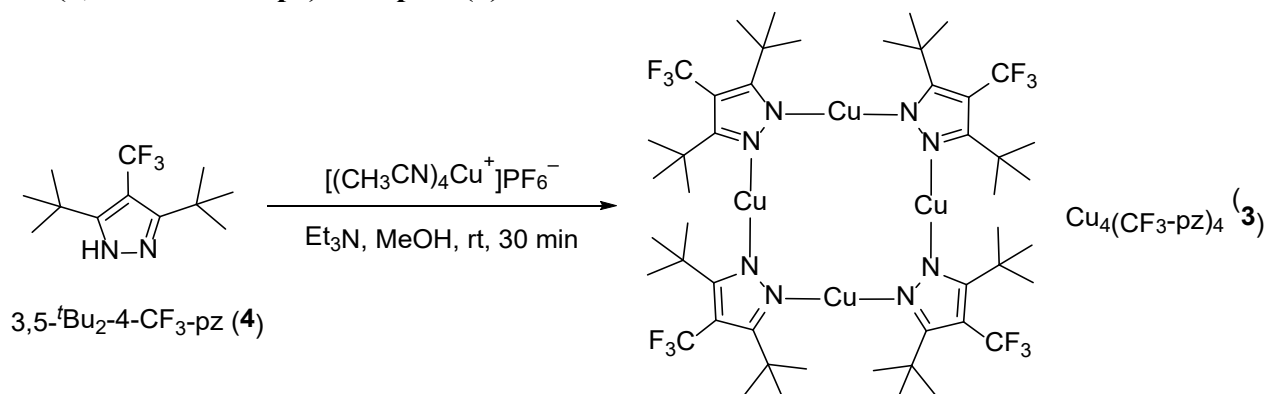
Methanol and triethylamine (Et$_3$N) were freshly distilled and degassed prior to use. CF$_3$-pyrazole **4** (100 mg, 0.4 mmol) was added to a flame-dried Schlenk flask with stir bar under argon and dissolved in pure methanol (4.5 mL). The solution was degassed with argon then treated with [(CH$_3$CN)$_4$Cu$^+$]PF$_6^-$ (150.1 mg, 0.4 mmol) and stirred for 5 minutes, followed by the dropwise addition of degassed Et$_3$N (224 μL, 1.6 mmol). The reaction mixture was stirred under argon for another 30 minutes to produce a precipitate, which was filtered, washed with methanol and hexanes, and dried under vacuum to yield Cu$_4$(CF$_3$-pz)$_4$ complex **3** as a colorless solid (81.0 mg, 64.7%). ^{1}H NMR (500 MHz, CDCl$_3$): δ 1.43 (s). ^{19}F NMR (101 MHz, CDCl$_3$): δ –45.3 (s). ^{13}C NMR (126 MHz, CDCl$_3$) δ 160.90, 128.29–121.93 (q, *J* 266.5 Hz), 106.13–105.25 (q, *J* 37.0 Hz), 33.34, 31.25. Anal calcd for C$_{48}$H$_{72}$Cu$_4$F$_{12}$N$_8$: C, 46.37; H, 5.84; N, 9.01; found: C, 46.63; H, 5.88; N: 8.91.

3. Photophysical characterization

I. Photoluminescence quantum yield and lifetime analysis of complex 3 (solid state)

The PL quantum yield (Φ_{PL}) is the ratio of the number of photons emitted (N_{em}) to the number of photons absorbed (N_{abs}). Spectral scans of the excitation scatter region (S_{ref}, S_A and S_B) and the emission regions of the reference and samples (A and B) (E_{ref}, E_A and S_B) were used to calculate Φ_{PL} by the direct and indirect excitation method, according to Equation S1:

$$\Phi_{PL} = \frac{N^{em}}{N^{abs}} = \frac{S_A(E_B - E_{ref.}) - S_B(E_A - E_{ref.})}{(S_A - S_B)S_{ref.}} \qquad (S1)$$

Sample A (E_A and S_A) spectral scan measurement: sample is excited directly. Sample B (E_B and S_B) spectral scan measurement: sample is excited indirectly by scattered photons in the spherical chamber. Excitation wavelength bandwidth ($\Delta\lambda_{ex}$) is 10 nm; emission wavelength bandwidth ($\Delta\lambda_{em}$) is 0.1 nm.

Thin-film samples (7 × 10 mm quartz substrates) were measured on 10-mm diameter trays made from PTFE with quartz coverlets that are part of the FLS 980's integrating sphere assembly. A same size quartz substrate was used as a reference.
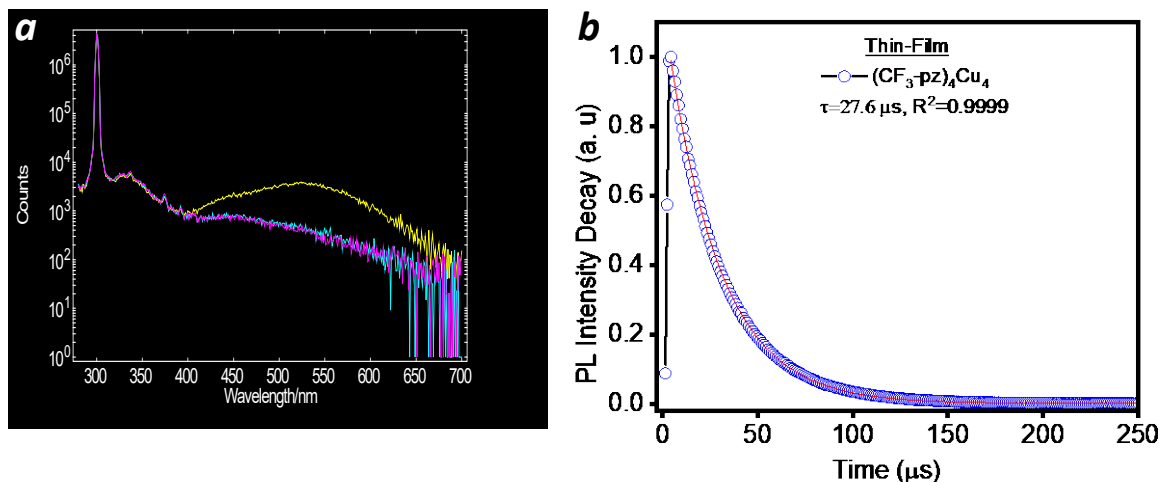
Figure S1. (a) Spectral scan of the excitation scatter and the emission region of Cu$_4$(CF$_3$-pz)$_4$ **3** (thin film) to calculate PL quantum yields. (b) Transient PL decay curve of Cu$_4$(CF$_3$-pz)$_4$ thin film at 300 K (λ_{ex} 270 nm), yielding a PL lifetime of 27.6 μs.

Table S1. Photophysical characteristics of Cu$_4$(CH$_3$-pz)$_4$ **2** and Cu$_4$(CF$_3$-pz)$_4$ **3** (thin film)

Cu$_4$pz$_4$ complex	Φ_{PL} [b]	λ_{em} [b] (nm)	FWHM (nm)	τ [b] (μs)	k_r [c] (s^{-1})	k_{nr} [d] (s^{-1})
Cu$_4$(CH$_3$-pz)$_4$ **2** [a]	0.78	461	65	15.2	5.13×10^4	1.45×10^4
Cu$_4$(CF$_3$-pz)$_4$ **3**	0.42	519[e]	125	27.6	1.52×10^4	2.1×10^4

[a] From Ref. S6. [b] Determined using an integrating sphere at 300 K. λ_{ex} = 300 nm for Cu$_4$(CH$_3$-pz)$_4$ **2** and 270 nm for Cu$_4$(CF$_3$-pz)$_4$ **3**. [c] $k_r = \Phi_{PL}/\tau$. [d] $k_{nr} = (1-\Phi_{PL})/\tau$. [e] Peak emission; see Fig. S5 for more information.

II. Absorption, emission, and excitation spectra of complex 3 (powder and thin film)
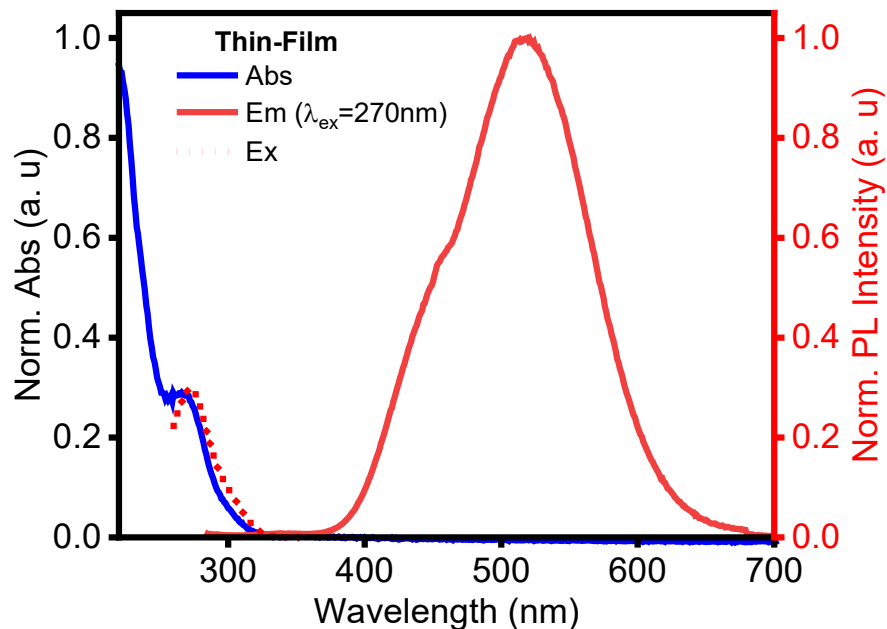
Figure S2. Normalized absorbance (blue), emission (λ_{ex} = 270 nm, solid red) and excitation (dotted red) spectra of $Cu_4(CF_3\text{-}pz)_4$ complex **3** in thin-film form at 297 K. The excitation spectra for λ_{em} @ 450 nm and 519 nm are nearly identical.
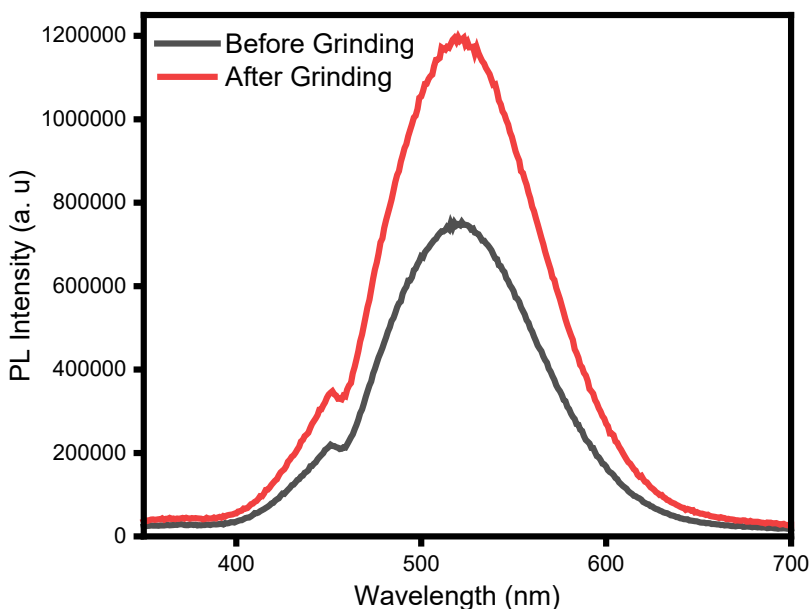
Figure S3. Emission spectrum of $Cu_4(CF_3\text{-}pz)_4$ powder before and after grinding (λ_{ex} = 270 nm). No changes in peak positions are observed.

III. Absorbance and photoluminescence spectra of complex 3 in CH_2Cl_2 (solution)
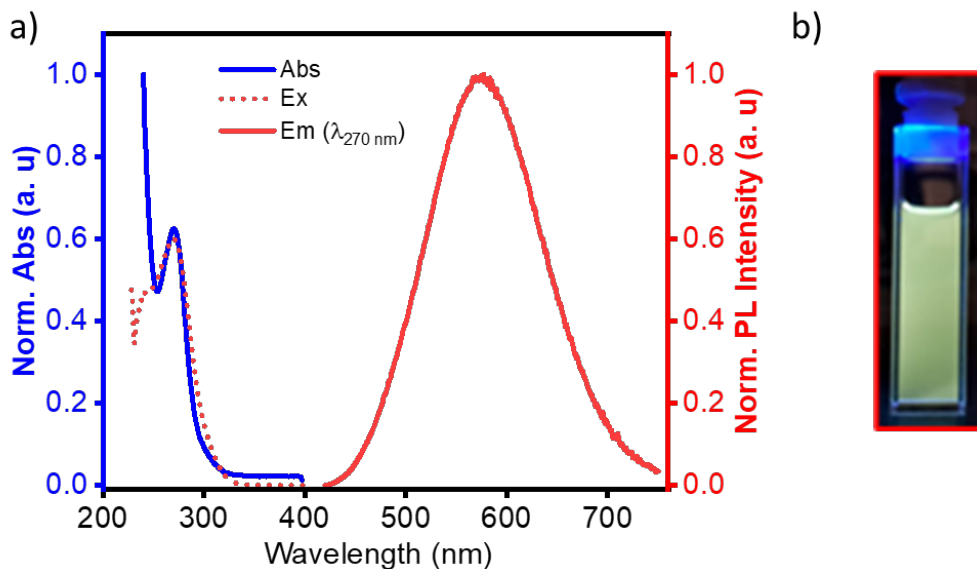
Figure S4. (a) Normalized absorbance (blue), emission (λ_{ex} = 270 nm, solid red) and excitation (dotted red) spectra of $Cu_4(CF_3\text{-}pz)_4$ complex **3** in solution (10 µM in CH_2Cl_2) at 297 K. (b) Luminescence of **3** in solution exposed to UV lamp (λ_{ex} = 254 nm).

The peak emission of **3** in solution (λ_{ex} 575 nm) is blueshifted by 25 nm relative to that of **2** in solution (λ_{em} 600 nm).[S7] This suggests that the conformation of **3** is more constrained due to the interdigitation of ^tBu groups between opposing pyrazolates, and that its persistence in the solution state is the result of steric crowding at the periphery of complex **3**.

IV. Variable-temperature photoluminescence spectra of complex 3 (solid state)
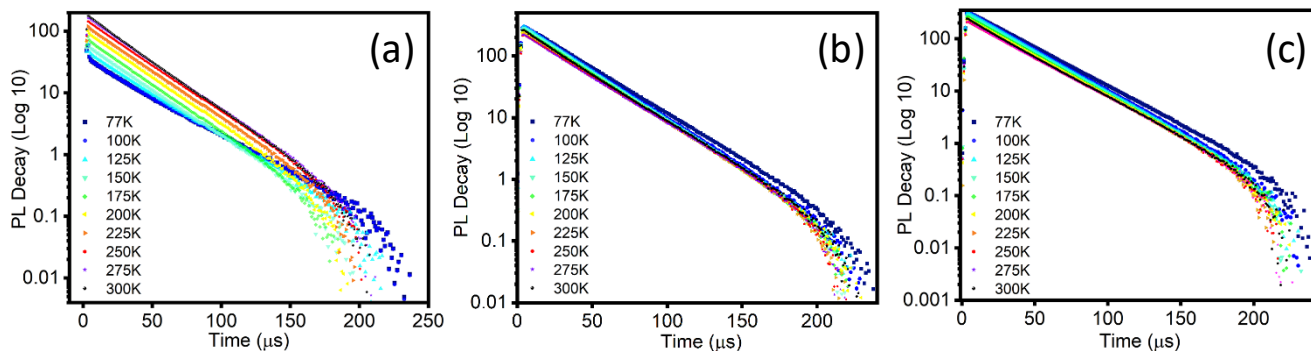
Figure S5. Variable-temperature PL timetime measurements of **3** in the solid state (thin film on quartz; λ_{ex} = 270 nm). (a) λ_{em} = 450 nm; (b) λ_{em} = 520 nm; (c) λ_{em} = 532 nm.

The PL lifetimes for **3** at 450 nm decrease modestly with rising temperature; $\tau_{450nm,77K}$ = 29.43 µs; $\tau_{450nm,300K}$ = 26.89 µs. PL lifetimes for **3** at 520 and 532 nm are temperature-insensitive; $\tau_{520nm,300K}$ = 27.56 µs; $\tau_{532nm,300K}$ = 29.82 µs.

4. Single-crystal X-ray crystallographic data

Single-crystal X-ray diffraction studies were carried out at the Purdue X-Ray Crystallography Facility using a Bruker AXS D8 Quest CMOS diffractometer. Single crystals of $Cu_4(CF_3\text{-}pz)_4$ complex **3** suitable for X-ray analyses were grown by slow solvent evaporation in dichloromethane/toluene mixture at room temperature. Crystals were coated with Fomblin oil (Solvay) and quickly transferred to the goniometer head of a Bruker Quest diffractometer with a fixed chi angle, a sealed tube fine focus X-ray tube, single crystal curved graphite incident beam monochromator, a Photon II area detector and an Oxford Cryosystems low temperature device. Examination and data collection were performed with Mo $K\alpha$ radiation ($\lambda = 0.71073$ Å) at 150 K and 200 K, with increased disorder observed at the latter temperature.

Reflections were indexed, scaled, and corrected for absorption using APEX3.[S8] Space groups were assigned and structures were solved by direct methods using XPREP within the SHELXTL suite of programs[S9] and refined by full matrix least squares against F^2 with all reflections using Shelxl2018 using the graphical interface Shelx.[S10,S11] H atoms were positioned geometrically and constrained to ride on their parent atoms, with carbon hydrogen bond distances of 0.95 Å for aromatic C–H and 0.99, and 0.98 Å for aliphatic CH_2 and CH_3 moieties, respectively. $U_{iso}(H)$ values were set to a multiple of $U_{eq}(C)$ with 1.2 for CH_2 and 1.5 for CH_3 units, respectively.

Complete crystallographic data in CIF format have been deposited with the Cambridge Crystallographic Data Centre. CCDC 2370077 and 2370073 contain the supplementary crystallographic data for this paper. These data can be obtained free of charge from the Cambridge Crystallographic Data Centre via www.ccdc.cam.ac.uk/data_request/cif.
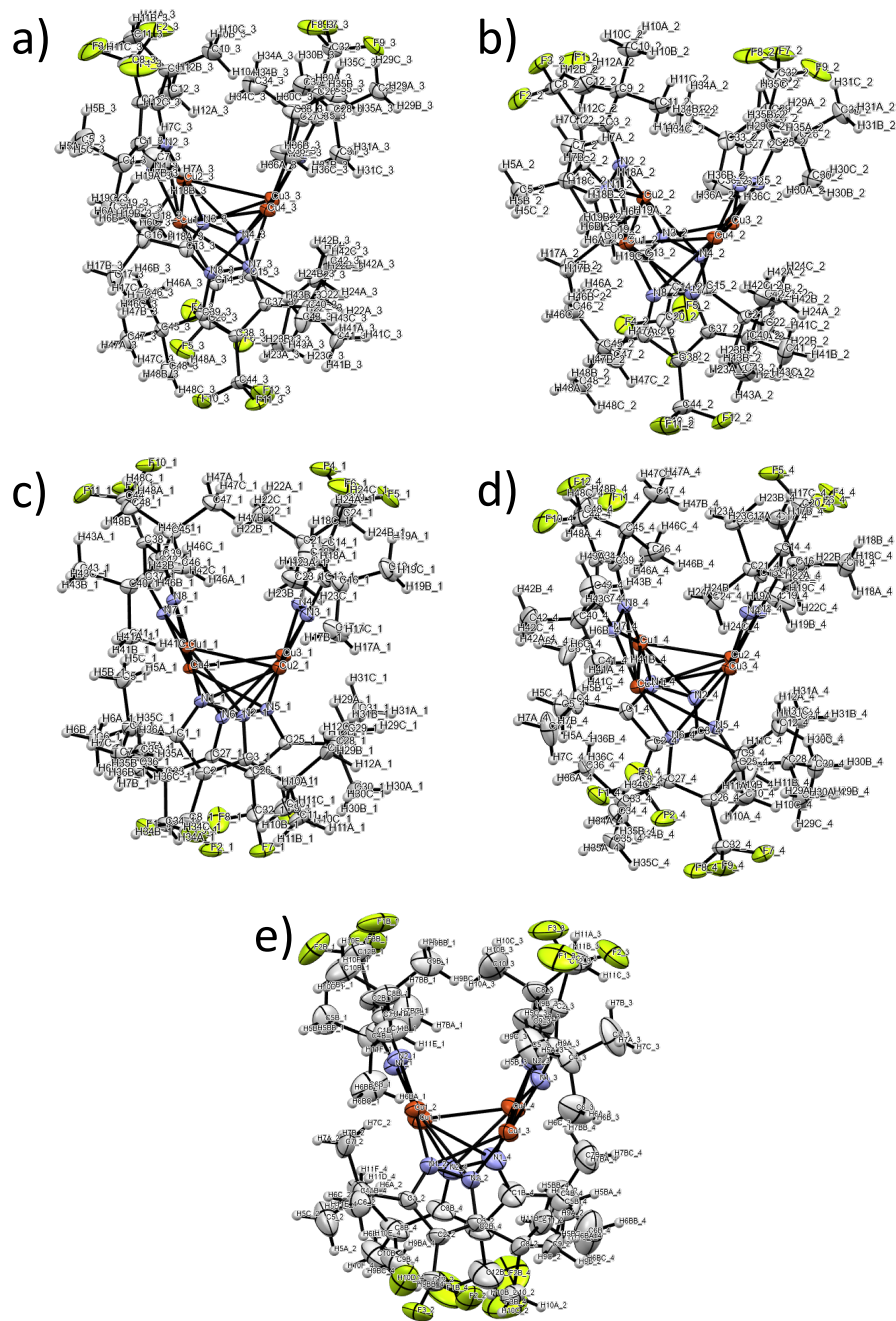
Figure S6. (a–d) ORTEP diagrams of conformers **I**, **II**, **III**, and **IV** of Cu$_4$(CF$_3$-pz)$_4$ complex **3** at 150 K (triclinic unit cell). (d) ORTEP diagram of **3** at 200 K (monoclinic unit cell). All structures were presented with thermal ellipsoids at 50% probability.

In the structure acquired at 200 K (**Figure S6d**), several CF$_3$ and ^{t}Bu groups occupy alternative geometries and contribute to disorder. ADPs of the methyl C atoms and trifluoromethyl F atoms are ill defined, however, the positions of all Cu atoms are completely ordered. ADPs of all atoms were restrained to be close to isotropic (ISOR 0.01 command of Shelxl) and were subjected to a rigid bond restraint (RIGU command of Shelxl). For the remaining disordered atoms, no restraints

for ADPs were applied. Subject to these conditions, the occupancy ratio for the ligand disorder is refined to 0.7579(13) to 0.2421(13). The final renderings are presented in **Figure S7**.

major pyrazole ligands
Occupancy ratio: 0.7579(13)

minor pyrazole ligands
Occupancy ratio: 0.2421(13)
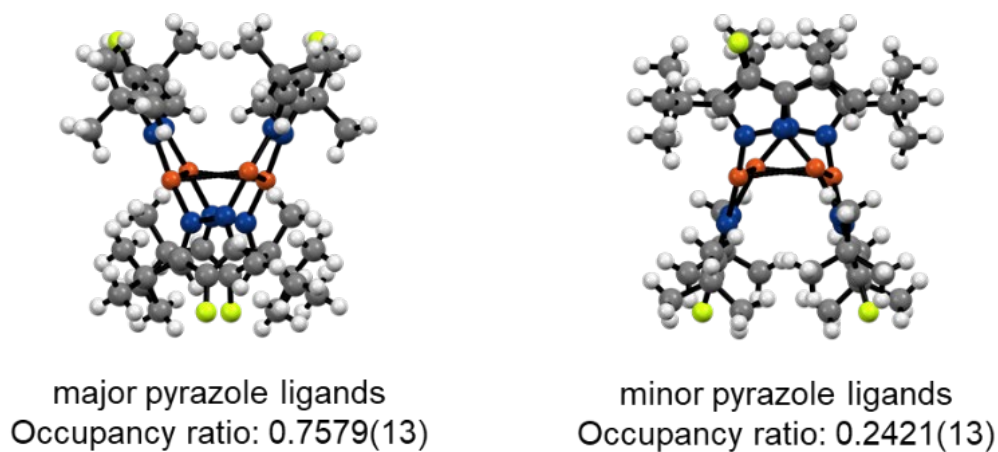
Figure S7. Major and minor geometries of $Cu_4(CF_3\text{-}pz)_4$ complex **3** at 200 K (static structures).
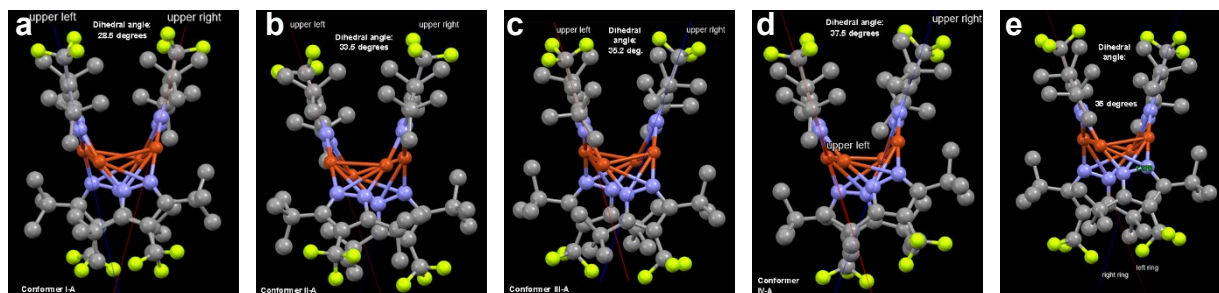
Figure S8. Ball-and stick models of complex **3**: (a–d) 150 K (Conformers **I–IV**); (e) 200 K. Each structure has a unique Cu_4 cluster geometry and set of dihedral angles formed by associated pyrazolate ligands.

Table S2. Various geometric parameters for $Cu_4(CF_3\text{-pz})_4$ complex **3** at 150 and 200 K. Data for $Cu_4(CH_3\text{-pz})_4$ complex **2** at 150 K (Ref. **Error! Bookmark not defined.**) added for comparison. Equivalent standard deviations (ESDs) for bond distances between adjacent Cu atoms are provided in parentheses.

	3-I (150 K)	3-II (150 K)	3-III (150 K)	3-IV (150 K)	3 (200 K)	2 (150 K)
Adjacent Cu···Cu distance (Å)	2.848(5)	2.834(6)	2.842(6)	2.807(5)	2.892(11)	2.857
	2.865(5)	2.910(5)	2.872(5)	2.829(5)	2.824(10)	2.878
	2.852(6)	2.821(6)	2.850(5)	2.832(6)	2.831(10)	2.856
	2.851(5)	2.836(5)	2.853(5)	2.897(5)	2.818(9)	2.882
Diagonal Cu···Cu distance (d_L and d_S, Å):	4.206	4.026	4.262	4.012	4.082	4.861
	3.711	3.901	3.654	3.901	3.814	3.046
Cu_4 quadrangle aspect ratio (d_L/d_S)	1.13	1.03	1.16	1.03	1.07	1.60
Cu_4 quadrangle bend angle (°)	27.4	28.8	32.9	29.2	28	< 1
Dihedral angles formed by planes of opposing pyrazolate ligands (°)	28.5	33.5	32.1	34.5	32.0	41.0
	34.7	36.0	35.2	37.5	35.0	42.7
Dihedral angle between N–N bonds of opposing pyrazolate ligands (°)	33.3	31.4	33.0	30.2	31.7	2.8
	33.8	34.3	33.1	32.5	34.0	4.4

Table S3. Crystal data and structure refinement for $Cu_4(CF_3\text{-pz})_4$ **3** at 150 K

Crystal data

Chemical formula	C48 H72 Cu4 F12 N8
Mr	1243.29
Crystal system, space group	Triclinic, 'P-1'
Temperature (K)	150
a, b, c (Å)	10.7542(15), 33.091(5), 33.101(6)
α, β, γ (°)	104.128(12), 95.625(12), 95.573(10)
V (Å^3)	11278(3)
Z	8
Radiation type	Mo $K\alpha$
μ (mm^{-1})	1.567
Crystal size (mm^3)	$0.380 \times 0.280 \times 0.170$

Data collection

Diffractometer	Bruker AXS D8 Quest with PhotonII charge-integrating pixel array (CPAD)
Absorption correction	Multi-scan SADABS 2016/2[S12]
T_{min}, T_{max}	0.587, 0.777
No. of measured, independent and observed [$I > 2\sigma(I)$] reflections	465628, 86222, 13341
R_{int}	0.0623
$(\sin \theta/\lambda)_{max}$ ranges (Å^{-1})	0.4050

Refinement

R [$F^2 > 2\sigma(F^2)$], $wR(F^2)$, S	0.0493, 0.1512, 1.081
No. of reflections	20516
No. of parameters	1099
H-atom treatment	H-atom parameters constrained
$\Delta\rho_{max}$, $\Delta\rho_{min}$ (e Å^{-3})	1.464, -0.758

Computer programs: Apex3 v2019.1-0, *SAINT* V8.40A (Ref. S8), *SHELXS97* (Ref. S9), *SHELXL2018*/3 (Ref. S10), SHELXLE Rev1030 (Ref. S11).

Table S4. Crystal data and structure refinement for $Cu_4(CF_3\text{-}pz)_4$ **3** at 200 K

Crystal data	
Chemical formula	C48 H72 Cu4 F12 N8
Mr	1243.29
Crystal system, space group	Monoclinic, 'P 21/c'
Temperature (K)	200
a, b, c (Å)	10.809(4), 26.109(10), 20.432(7)
α, β, γ (°)	90, 98.96(2), 90
V (Å^3)	5696(3)
Z	4
Radiation type	Mo $K\alpha$
μ (mm^{-1})	1.551
Crystal size (mm^3)	0.480×0.380×0.310
Data collection	
Diffractometer	Bruker AXS D8 Quest with PhotonII charge-integrating pixel array (CPAD)
Absorption correction	Multi-scan SADABS 2016/2[S12]
T_{min}, T_{max}	0.523, 0.645
No. of measured, independent and observed [$I > 2\sigma(I)$] reflections	82366, 20516
R_{int}	0.0398
$(\sin\theta/\lambda)_{max}$ ranges (Å^{-1})	0.4050
Refinement	
R [$F^2 > 2\sigma(F^2)$], $wR(F^2)$, S	0.0272, 0.0734, 1.039
No. of reflections	86222
No. of parameters	2690
H-atom treatment	H-atom parameters constrained
$\Delta\rho_{max}, \Delta\rho_{min}$ (e Å^{-3})	1.137, −1.191

Computer programs: Apex3 v2019.1-0, *SAINT* V8.40A (Ref. S8), *SHELXS97* (Ref. S9), *SHELXL2018*/3 (Ref. S10), SHELXLE Rev1030 (Ref. S11).

5. Theoretical (TD-DFT) calculations

Coordinates from the crystal structure of $Cu_4(CF_3\text{-}pz)_4$ complex **3** (150 K) were used in the initial geometries for calculations, which were fully optimized at the PBE0/TZVP level for H, C, N, F, and Cu atoms, with ECP calculations for Cu.
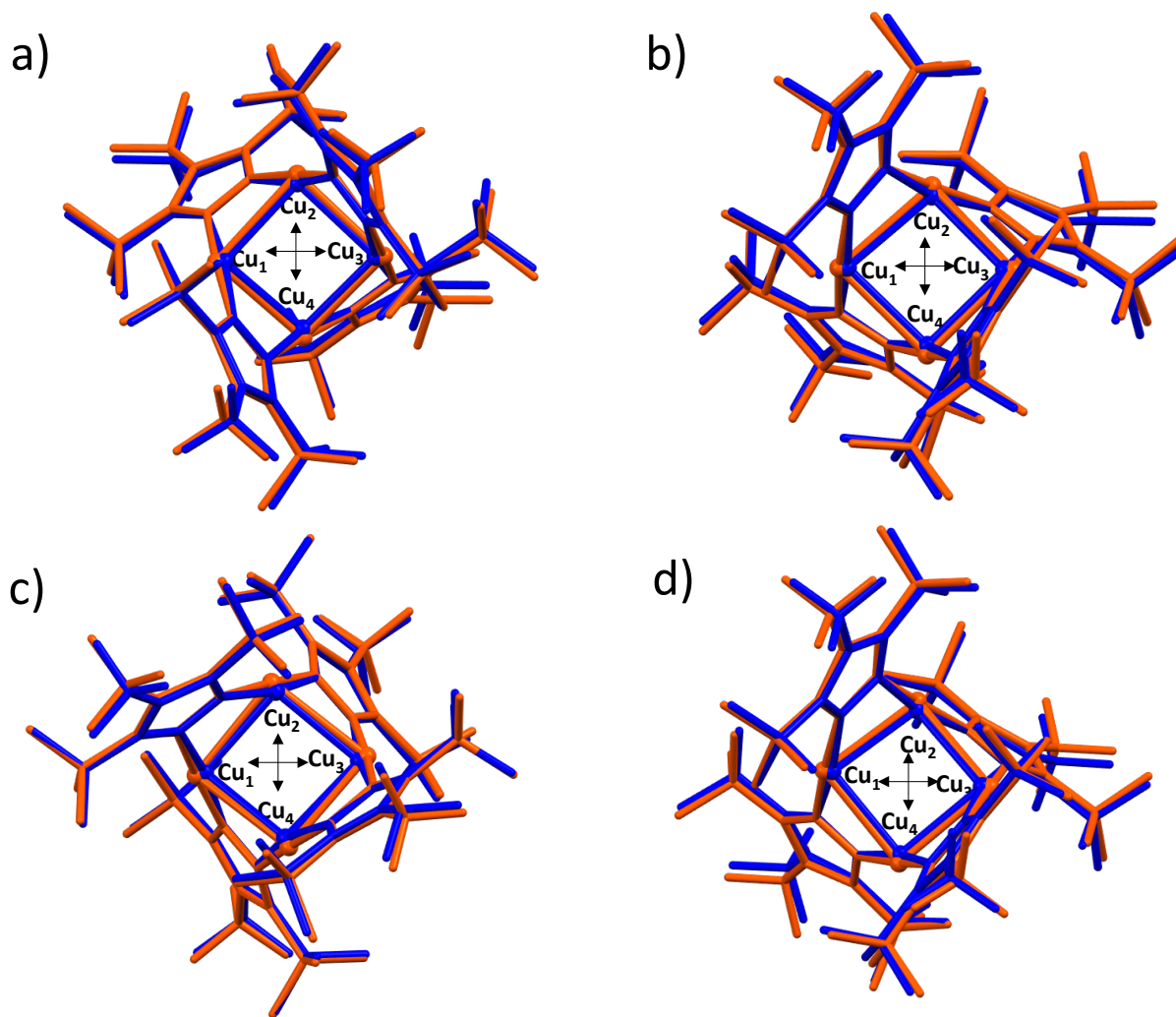
Figure S9. (a) TD-DFT excited-state conformational analysis of conformers **I–IV** for $Cu_4(CF_3\text{-}pz)_4$ complex **3**, with optimized geometries of their initial S_0 (orange) states and final excited-state conformations in their T_1 (blue) states. All hydrogen atoms are omitted for clarity.
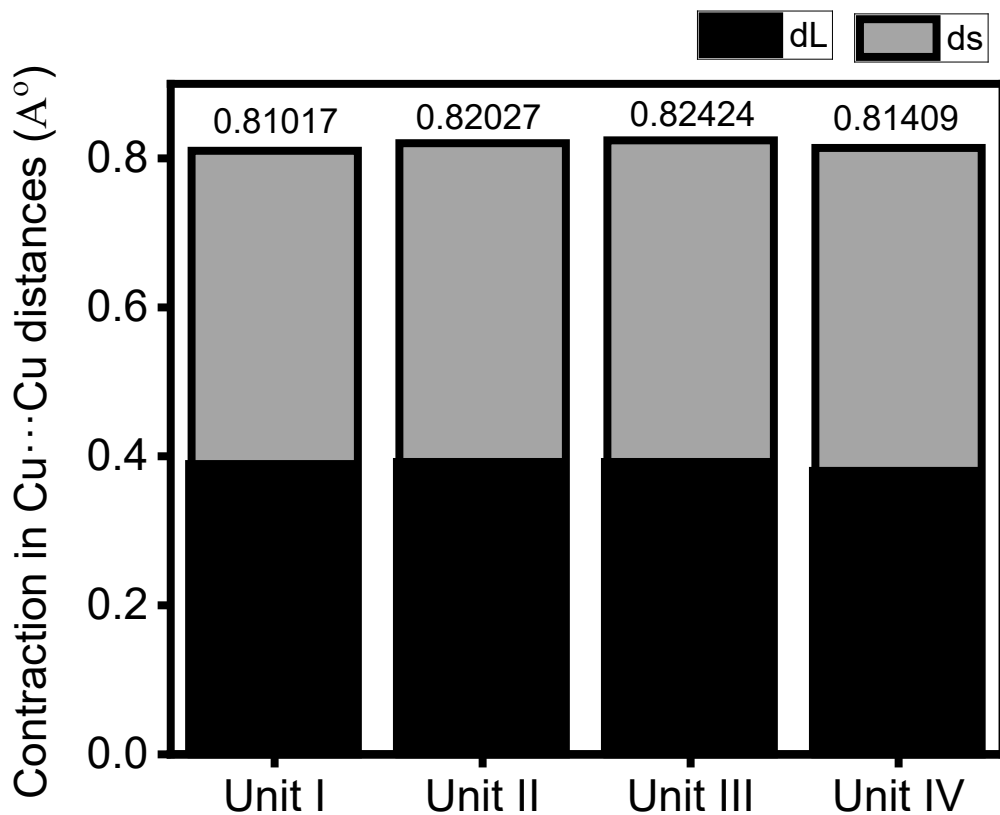
Figure S10. Parameterized excited-state contraction of the Cu_4 cores between the S_0 and T_1 states of conformers **I–IV**. Light and dark grey bars represent decreases in the Cu⋯Cu distances along d_S (Cu_1⋯Cu_3) and d_L (Cu_2⋯Cu_4) axes respectively.

Table S5. $S_0 \rightarrow T_1$, T_2 and $S_0 \rightarrow S_1$, S_2 transitions, energies (E_{calc}), and orbital contributions for Cu₄pz₄ complexes **2** and **3** (Conformers **I–IV**) from TD-DFT calculations.

Cu₄pz₄ complex	State	E_{calc} (eV)	Orbital contribution
2 (R = CH₃)[Error! Bookmark not defined.]	T_1	3.60	HOMO-5→LUMO (23%) HOMO-1→LUMO (75%) HOMO→LUMO (2%)
	T_2	3.66	HOMO→LUMO (100%)
	S_1	4.43	HOMO→LUMO (100%)
	S_2	4.54	HOMO-5→LUMO (19%) HOMO-1→LUMO (81%)
3 (R = CF₃) **Conformer I** −ΔH_f: **2690240.68 kcal/mol** **(reference ΔH_0)**	T_1	3.51	HOMO→LUMO (100%)
	T_2	3.95	HOMO-8→LUMO (14.4%) HOMO-1→LUMO (55.1%) HOMO→LUMO+1 (30.5%)
	S_1	4.35	HOMO→LUMO (100%)
	S_2	4.88	HOMO-1→LUMO (100%)
3 (R = CF₃) **Conformer II** −ΔH_f: **2690239.70 kcal/mol** ΔΔH_f: **−0.98 kcal/mol**	T_1	3.52	HOMO→LUMO (100%)
	T_2	3.96	HOMO-1→LUMO (100%)
	S_1	4.37	HOMO→LUMO (100%)
	S_2	4.88	HOMO-1→LUMO (100%)
3 (R = CF₃) **Conformer III** −ΔH_f: **2690239.71 kcal/mol** ΔΔH_f: **−0.97 kcal/mol**	T_1	3.52	HOMO→LUMO (100%)
	T_2	3.96	HOMO-2→LUMO (16.9%) HOMO-1→LUMO (83.1%)
	S_1	4.37	HOMO→LUMO (100%)
	S_2	4.88	HOMO-1→LUMO (100%)
3 (R = CF₃) **Conformer IV** −ΔH_f: **2690240.69 kcal/mol** ΔΔH_f: **+0.01 kcal/mol**	T_1	3.51	HOMO→LUMO (100%)
	T_2	3.95	HOMO-2→LUMO (44.7%) HOMO-1→LUMO (55.2%)
	S_1	4.35	HOMO→LUMO (100%)
	S_2	4.88	HOMO-1→LUMO (100%)

Table S6. Excited-state (T_1) geometry optimizations of $Cu_4(CF_3\text{-}pz)_4$ complexes from TD-DFT calculations.

Cu_4pz_4 complex	State	f	E_{calc} (λ)	Orbital contribution
1	T_1 (opt)	0	2.44 eV (508 nm)	HOMO-9→LUMO (8%) HOMO-8→LUMO (5%) HOMO-4→LUMO (12%) HOMO→LUMO (75%)
3-I	T_1 (opt)	0	2.72 eV (456 nm)	HOMO→LUMO (100%)
3-II	T_1 (opt)	0	2.73 eV (453 nm)	HOMO→LUMO (100%)
3-III	T_1 (opt)	0	2.74 eV (453 nm)	HOMO→LUMO (100%)
3-IV	T_1 (opt)	0	2.72 eV (456 nm)	HOMO→LUMO (100%)

Table S7. Contraction of Cu···Cu distances between ground state (S_0) and excited state (T_1) for $Cu_4(CF_3-pz)_4$ conformers **3-I** through **3-IV**, optimized by TD-DFT calculations.

$Cu_4(CF_3-pz)_4$ conformer	Diagonal axis	State	Distance (d) (Å)	Δd (Å)	Total Cu···Cu contraction ($\Delta d_S + \Delta d_L$)
3-I	$Cu_1 \cdots Cu_3$ (d_S)	Ground (S_0)	3.94090	0.42428	0.81017
		Triplet (T_1)	3.51662		
	$Cu_2 \cdots Cu_4$ (d_L)	Ground (S_0)	3.99140	0.38589	
		Triplet (T_1)	3.60551		
3-II	$Cu_1 \cdots Cu_3$ (d_S)	Ground (S_0)	3.90131	0.44352	0.82027
		Triplet (T_1)	3.45779		
	$Cu_2 \cdots Cu_4$ (d_L)	Ground (S_0)	4.02798	0.37675	
		Triplet (T_1)	3.65123		
3-III	$Cu_1 \cdots Cu_3$ (d_S)	Ground (S_0)	3.89313	0.43556	0.82424
		Triplet (T_1)	3.45757		
	$Cu_2 \cdots Cu_4$ (d_L)	Ground (S_0)	4.04039	0.38868	
		Triplet (T_1)	3.65171		
3-IV	$Cu_1 \cdots Cu_3$ (d_S)	Ground (S_0)	3.93735	0.41794	0.81409
		Triplet (T_1)	3.51941		
	$Cu_2 \cdots Cu_4$ (d_L)	Ground (S_0)	4.00018	0.39615	
		Triplet (T_1)	3.60403		

6. Differential scanning calorimetry
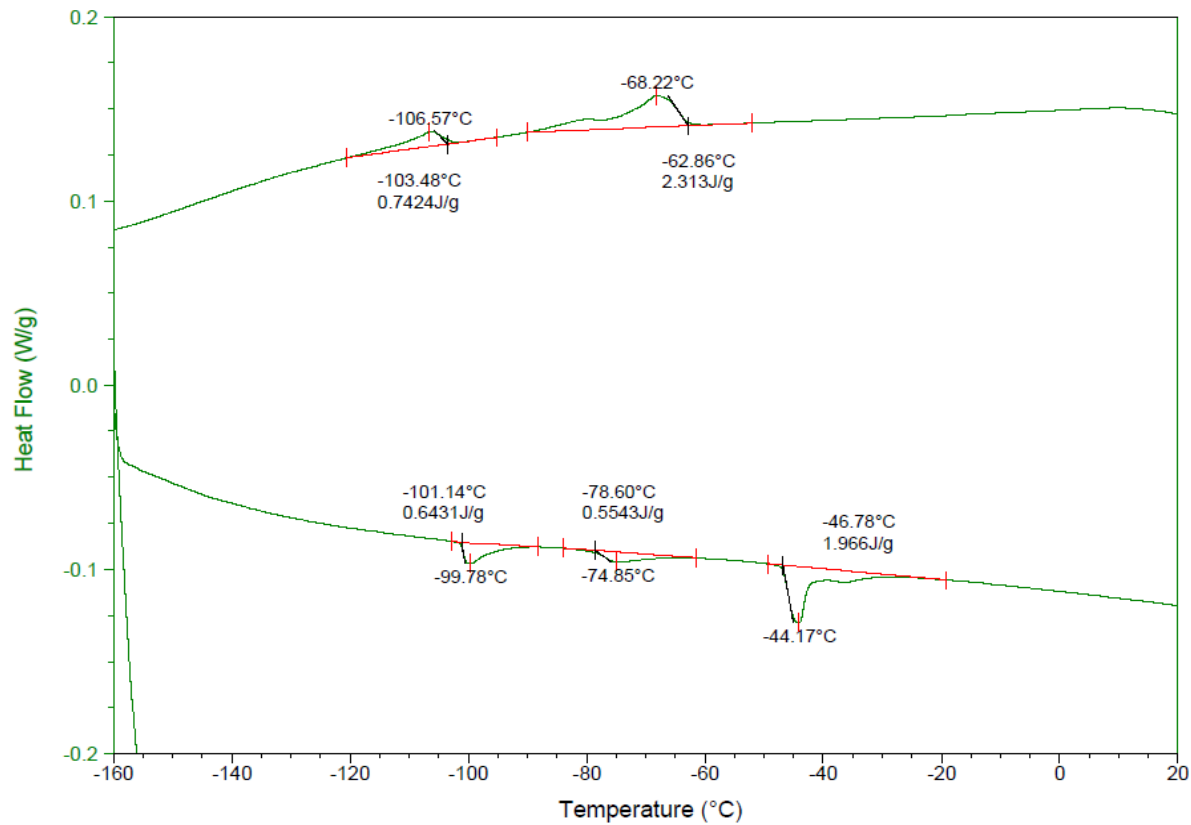
Figure S11. Differential scanning calorimetry of recrystallized $Cu_4(CF_3\text{-pz})_4$ complex **3.**

7. NMR spectra
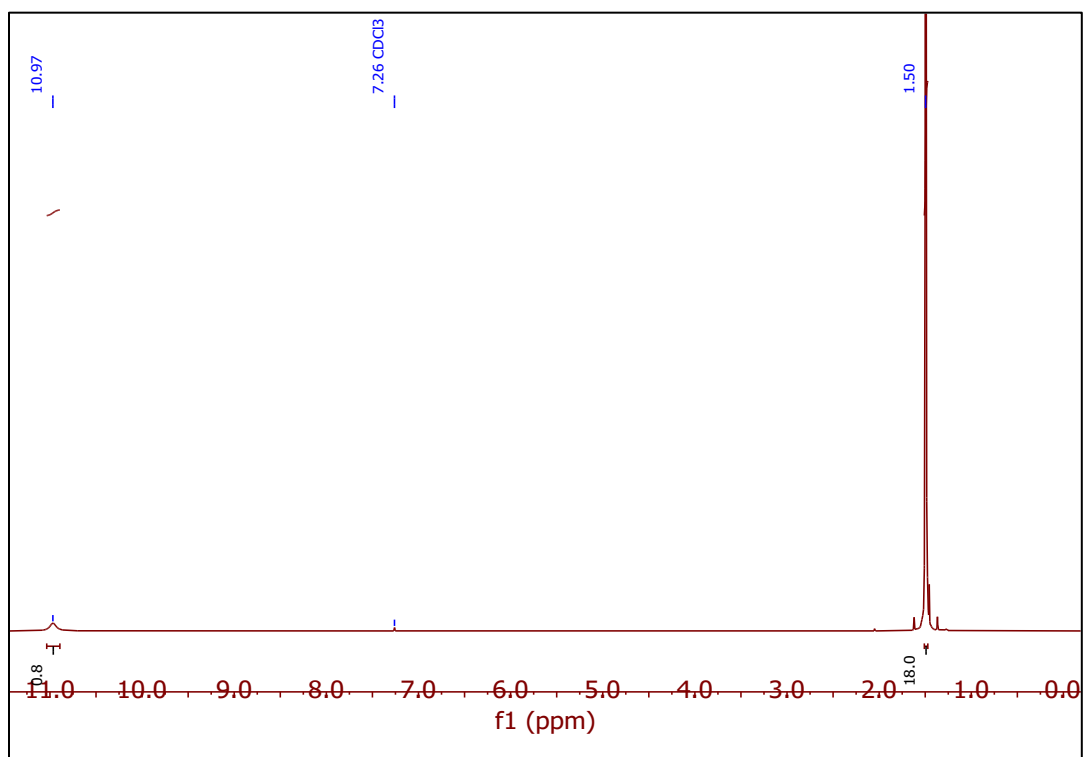
Figure S12. ^1H NMR spectrum of 3,5-$^tBu_2$-4-iodopyrazole (500 MHz, CDCl$_3$).
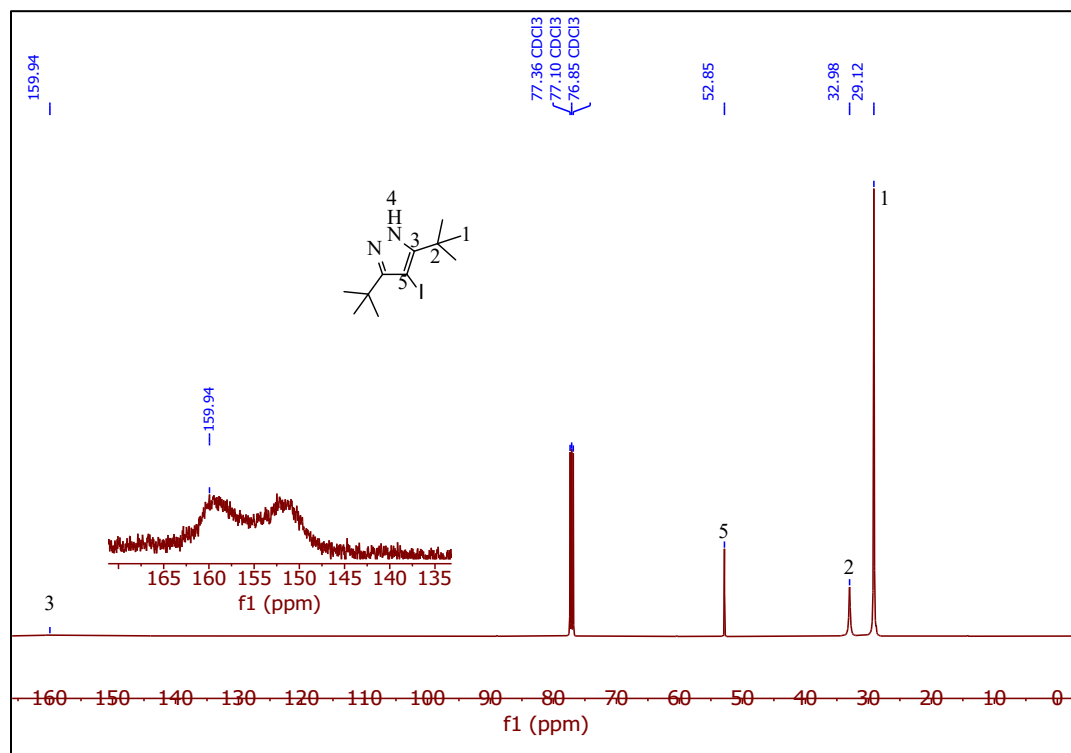
Figure S13. ^{13}C NMR spectrum of 3,5-$^tBu_2$-4-iodopyrazole (125 MHz, CDCl$_3$).
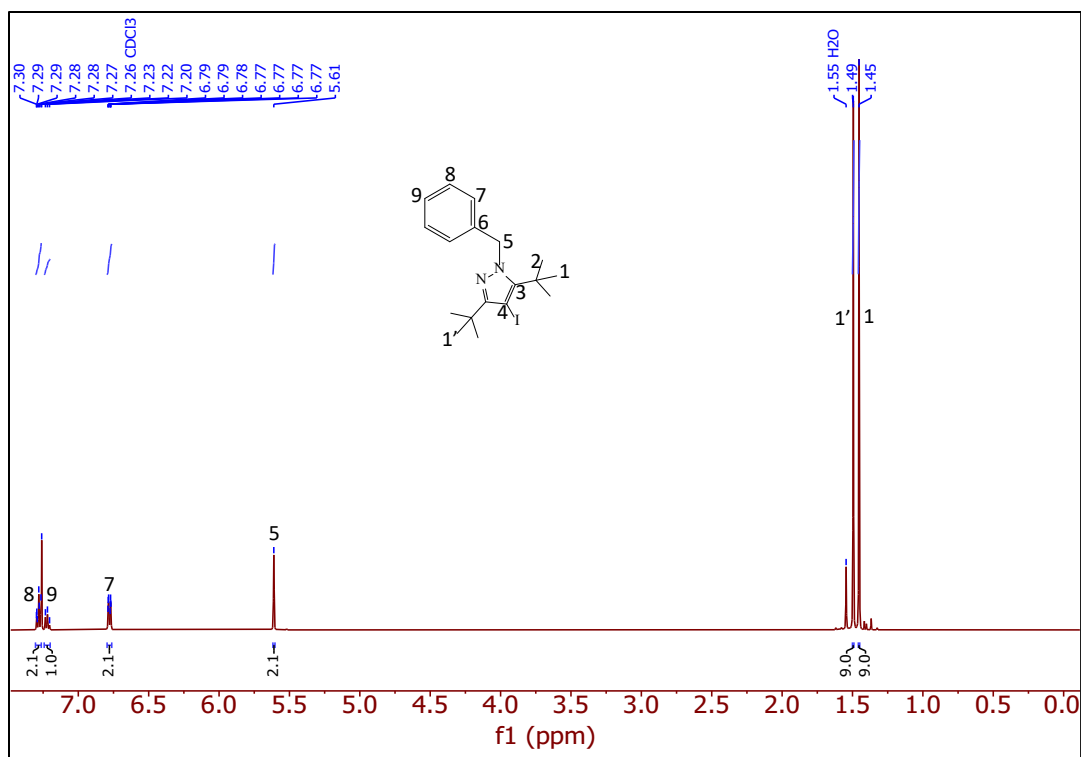
Figure S14. ^{1}H NMR spectrum of 1-benzyl-3,5-^{t}Bu$_2$-4-iodopyrazole (500 MHz, CDCl$_3$).
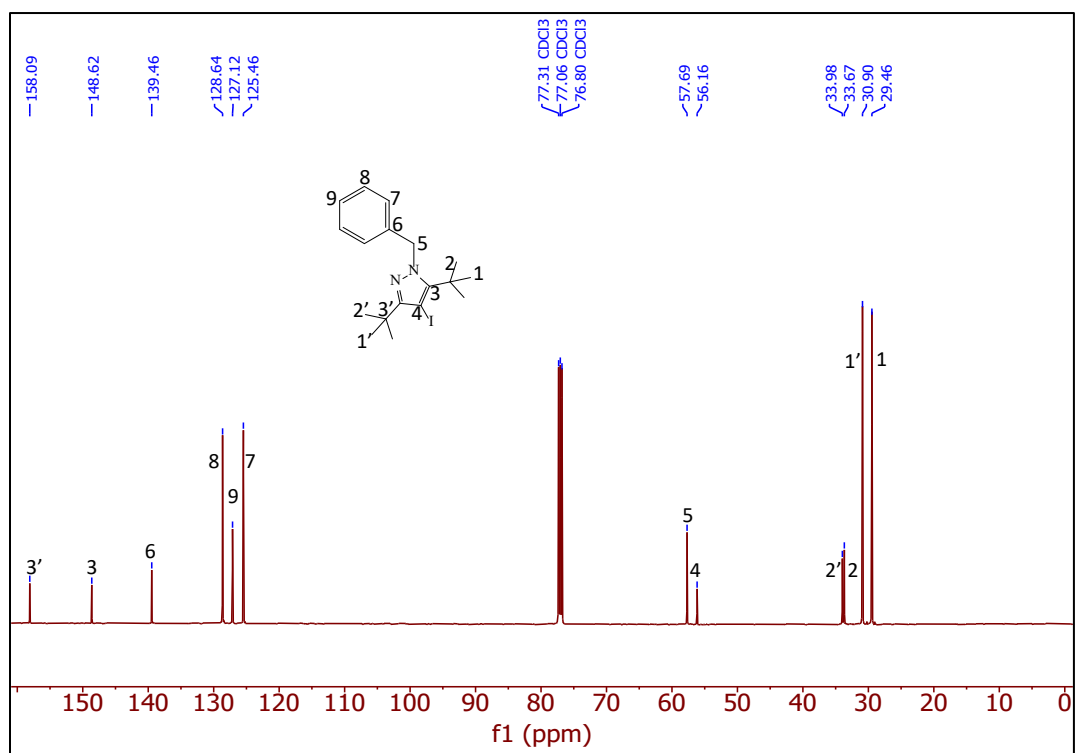
Figure S15. ^{13}C NMR spectrum of 1-benzyl-3,5-^{t}Bu$_2$-4-iodopyrazole (125 MHz, CDCl$_3$).
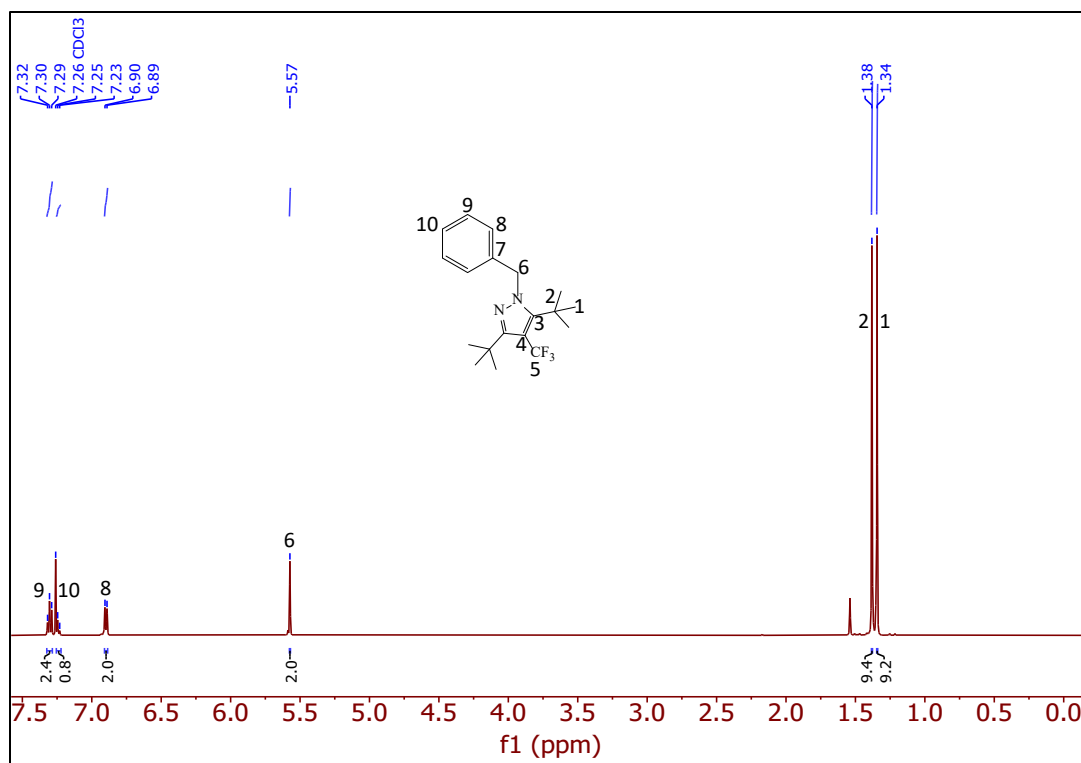
Figure S16. ^{1}H NMR spectrum of 1-benzyl-3,5-^{t}Bu$_2$-4-CF$_3$-pyrazole (500 MHz, CDCl$_3$).
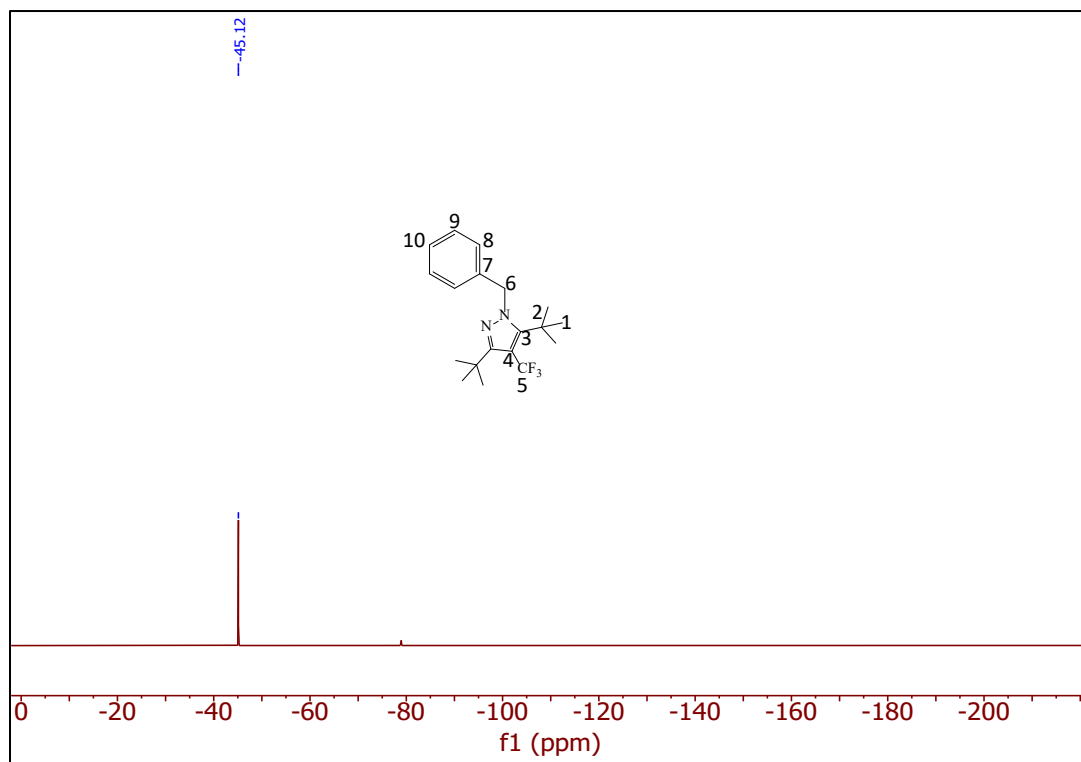
Figure S17. ^{19}F NMR spectrum of 1-benzyl-3,5-^{t}Bu$_2$-4-CF$_3$-pyrazole (376 MHz, CDCl$_3$).
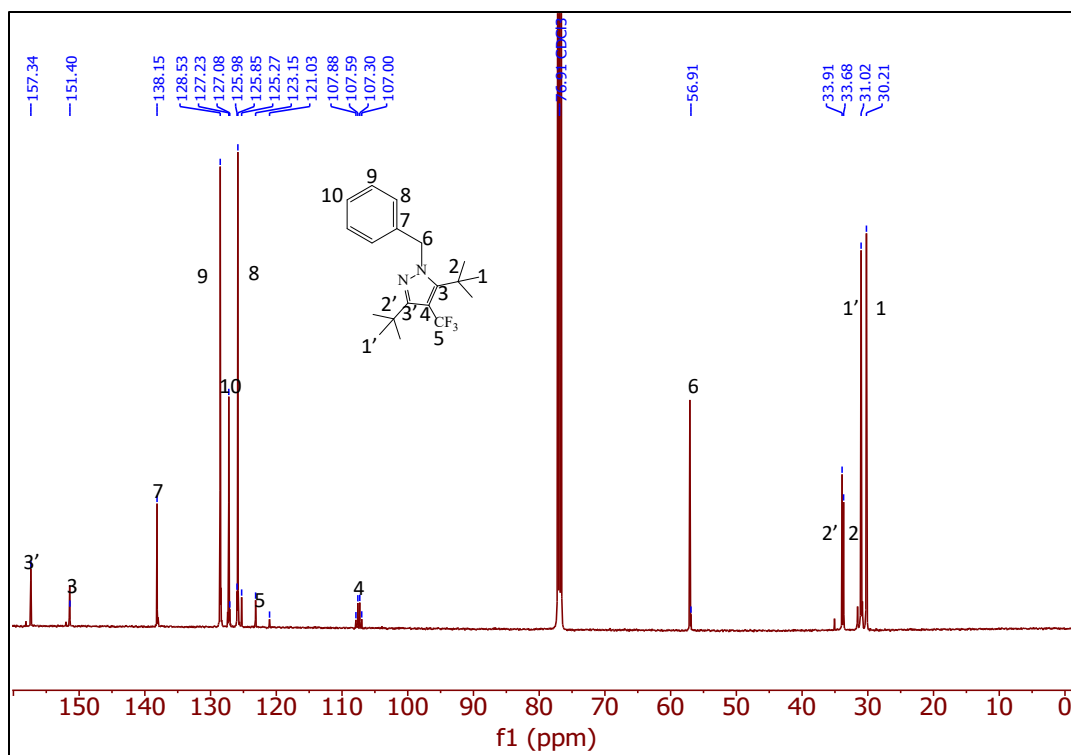
Figure S18. ^{13}C NMR spectrum of 1-benzyl-3,5-^{t}Bu$_2$-4-CF$_3$-pyrazole (125 MHz, CDCl$_3$).
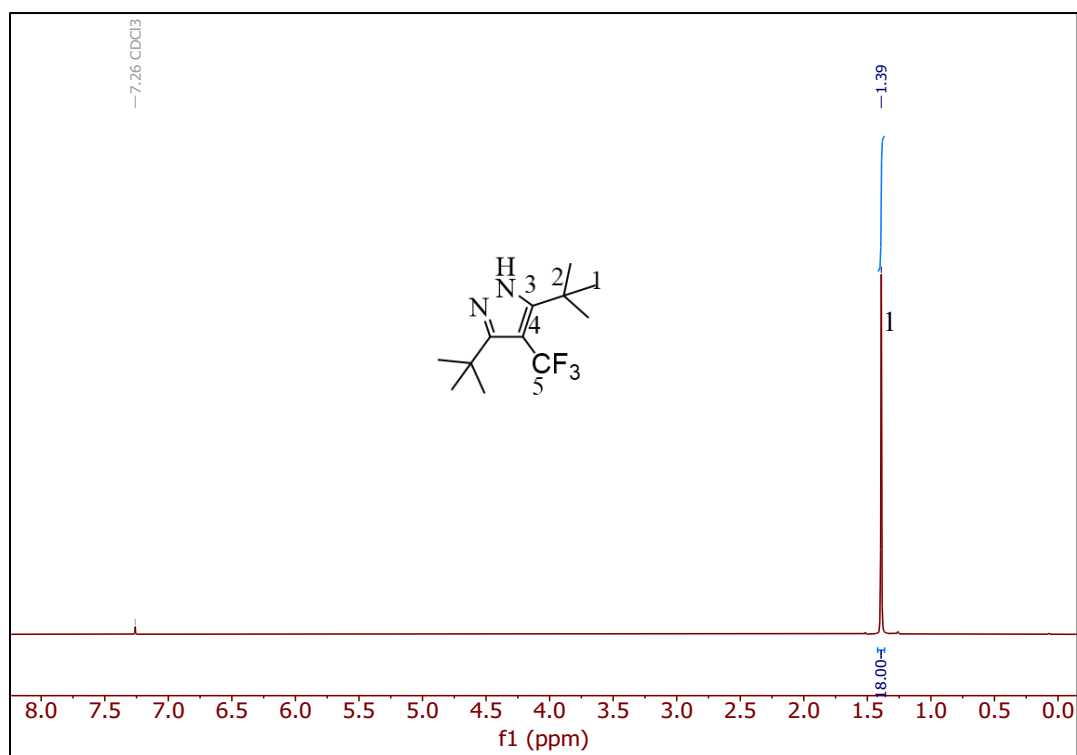
Figure S19. ^{1}H NMR spectrum of 3,5-^{t}Bu$_2$-4-CF$_3$-pyrazole **4** (500 MHz, CDCl$_3$).
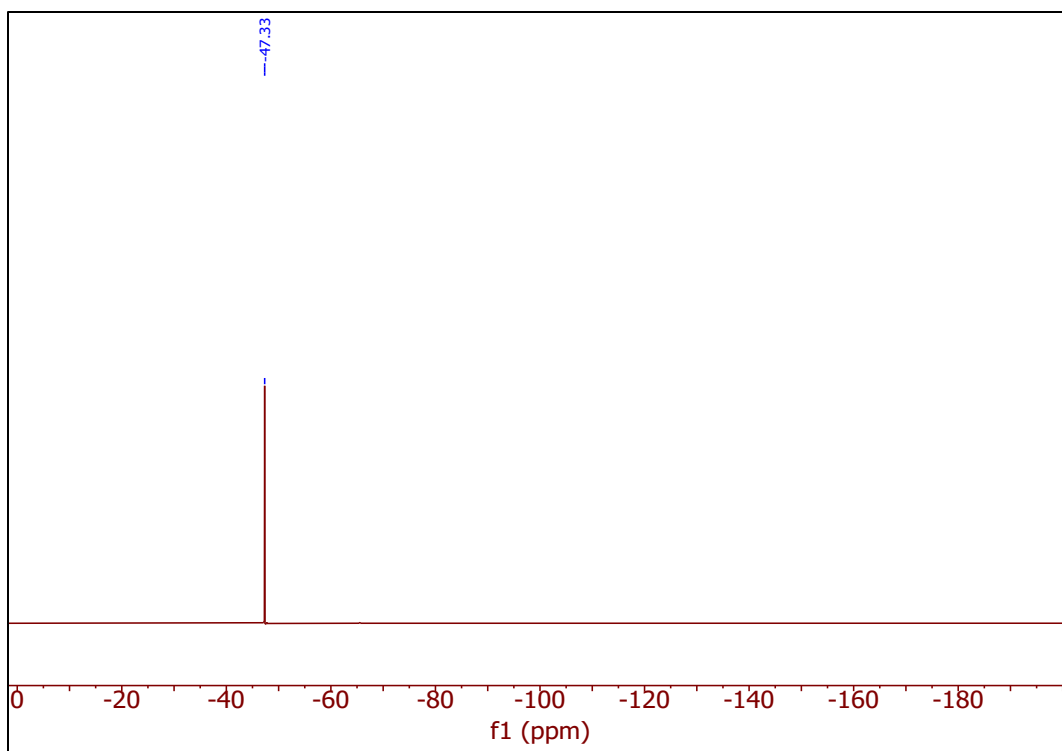
Figure S20. ^{19}F NMR spectrum of 3,5-$^{t}Bu_2$-4-CF_3-pyrazole **4** (376 MHz, CDCl$_3$).
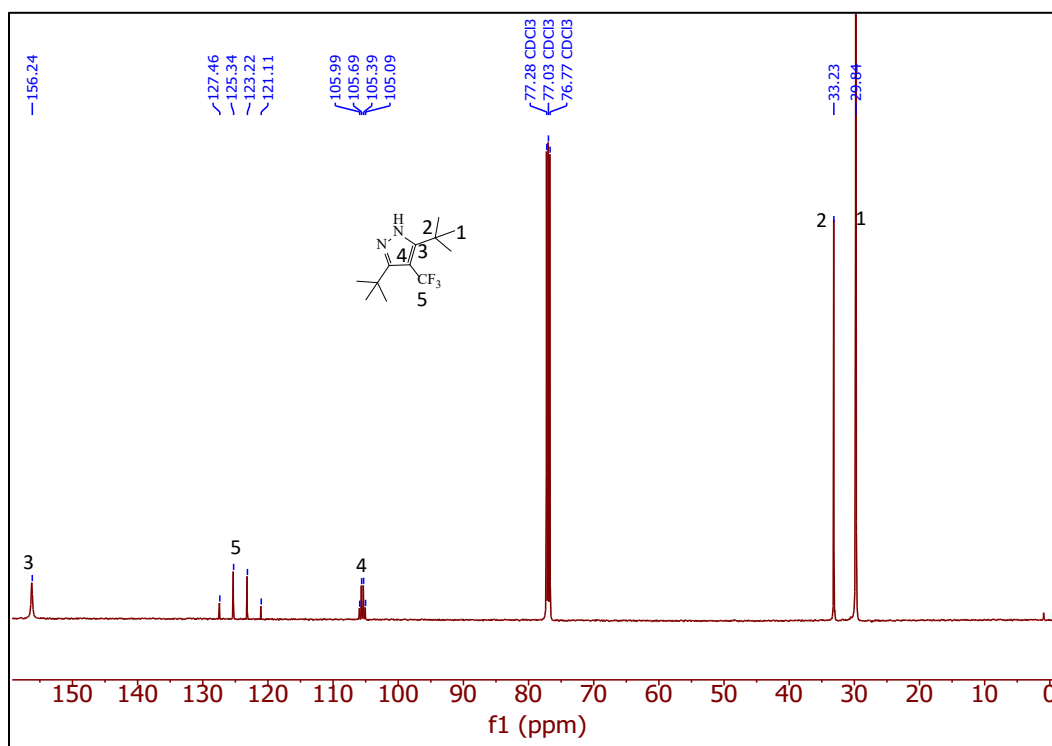
Figure S21. ^{13}C NMR spectrum of 3,5-$^{t}Bu_2$-4-CF_3-pyrazole **4** (100 MHz, CDCl$_3$).
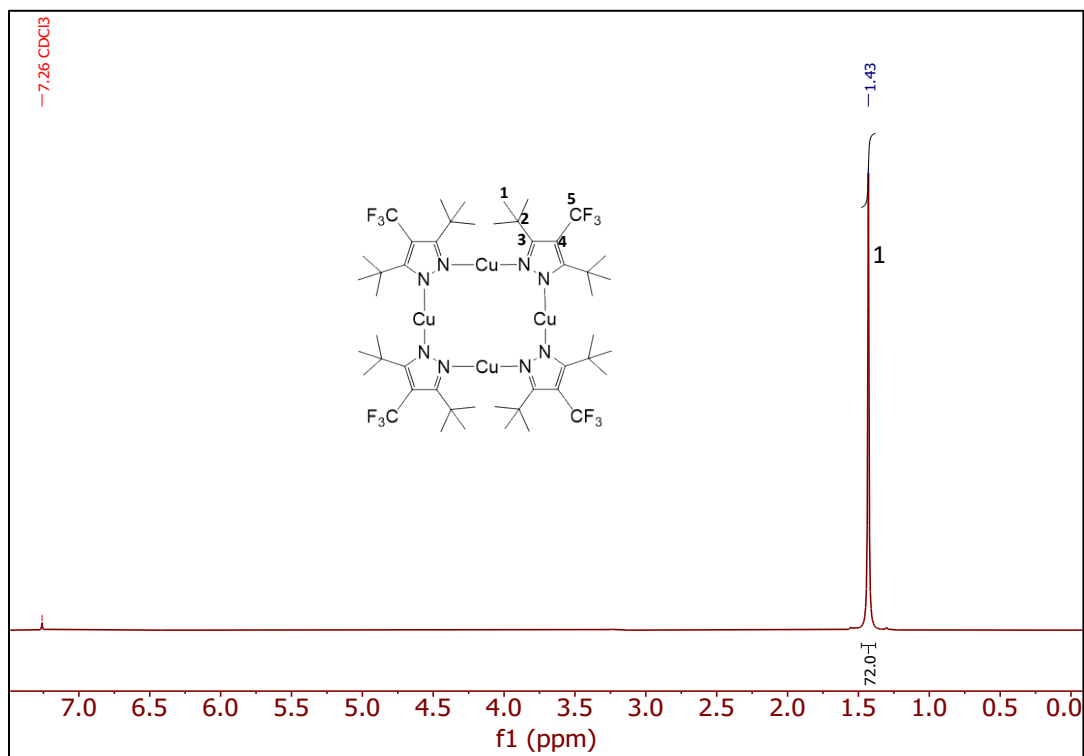
Figure S22. ^{1}H NMR spectrum of $Cu_4(CF_3\text{-pz})_4$ **3** (500 MHz, CDCl$_3$).
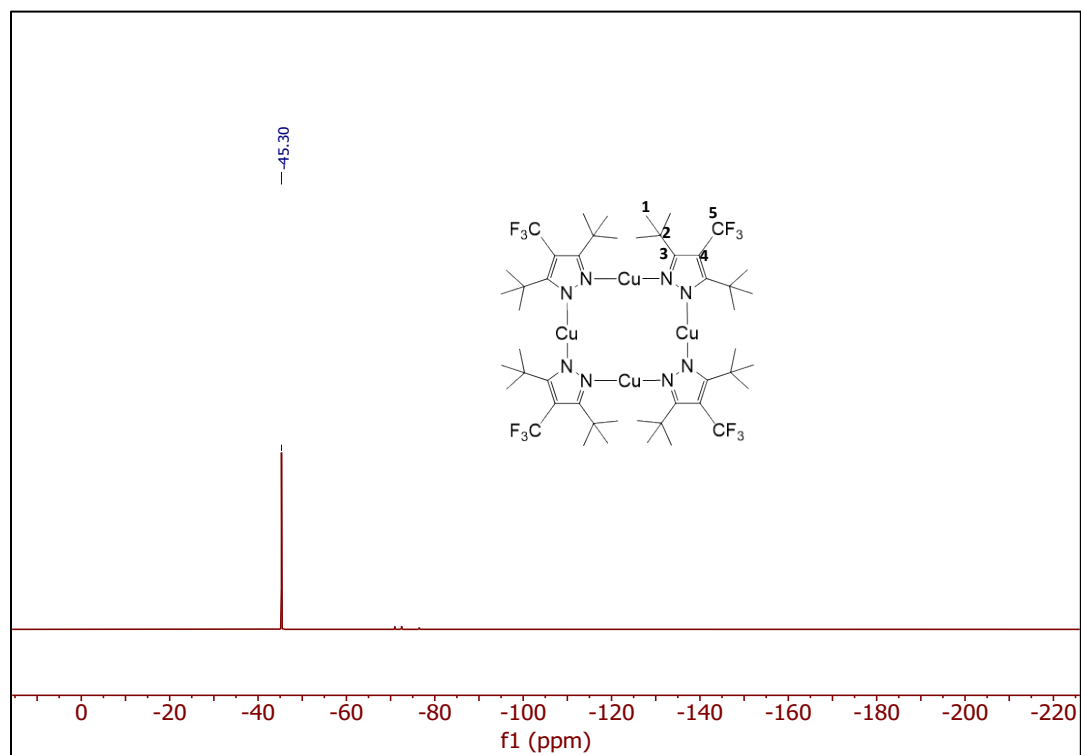
Figure S23. ^{19}F NMR spectrum of $Cu_4(CF_3\text{-pz})_4$ **3** (376 MHz, CDCl$_3$).
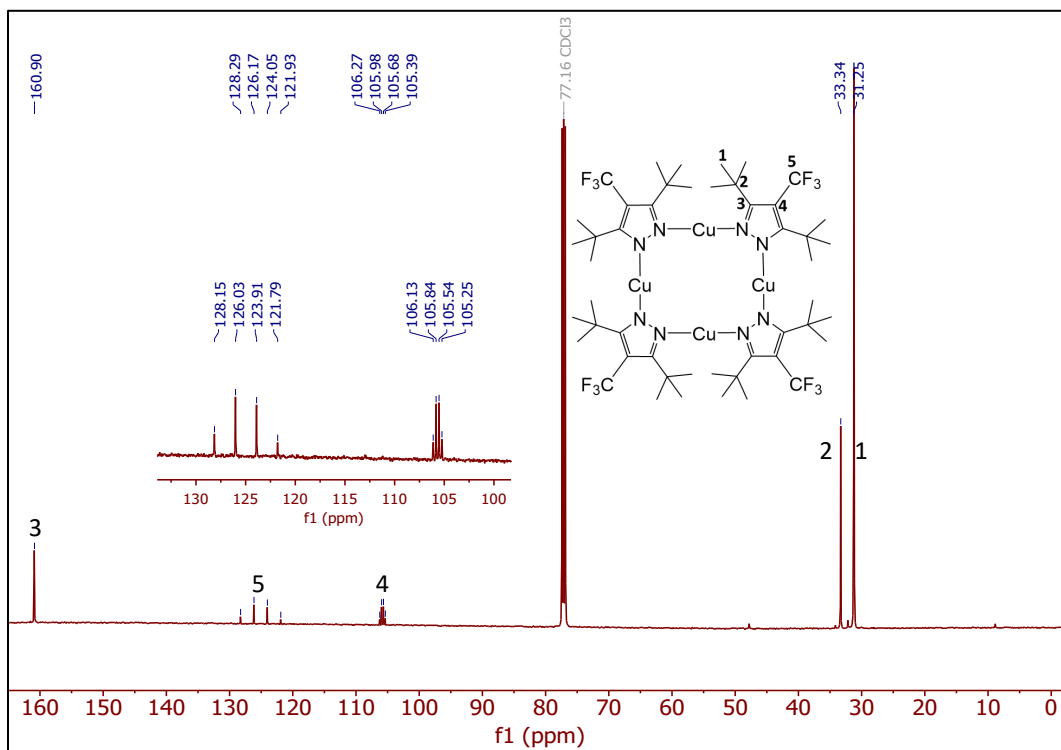
Figure S24. ^{13}C NMR spectrum of $Cu_4(CF_3\text{-pz})_4$ **3** (125 MHz, $CDCl_3$).

8. References

S1. M. J. Frisch, G. W. Trucks, H. B. Schlegel, G. E. Scuseria, M. A. Robb, J. R. Cheeseman, G. Scalmani, V. Barone, G. A. Petersson, H. Nakatsuji, et al., Gaussian 16 Rev. A.03, Gaussian, Inc., Wallingford, CT (2016).

S2. Siddiqui, A. M.; Ciblat, S.; Dery, M.; Constantineua-Forget, L.; Grand-Maitre, C.; Bruneau-Latour, N.; Shipps, G. W.; Cooper, A. B.; Oza, V.; Kostura, M. W.; Luther, M.; Levine, J., WO2018102453 A1 (2018).

S3. Stibrany, R. T.; Potenza, J. A., *J. Chem. Crystallogr.* **2009**, *39* (4), 266-269.

S4. Jia, H.; Häring, A. P.; Berger, F.; Zhang, L.; Ritter, T., *J. Am. Chem. Soc.* **2021**, *143* (20), 7623-7628.

S5. Rouse, M. B.; Seefeld, M. A., WO2010093885 A1 (2010).

S6. Watanabe, Y.; Washer, B. M.; Zeller, M.; Savikhin, S.; Slipchenko, L. V.; Wei, A., *J. Am. Chem. Soc.* **2022**, *144* (23), 10186-10192.

S7. (a) Wrighton, M.; Morse, D. L., *J. Am. Chem. Soc.* **1974**, *96* (4), 998-1003; (b) Kotch, T. G.; Lees, A. J.; Fuerniss, S. J.; Papathomas, K. I.; Snyder, R. W., *Inorg. Chem.* **1993**, *32* (11), 2570-2575.

S8. Bruker (**2019**). Apex3 v2019.1-0, S. V. A., Bruker AXS Inc.: Madison (WI), USA,; 2013/2014.

S9. (a) SHELXTL suite of programs, V., 2000-2003, Bruker Advanced X-ray Solutions, Bruker AXS Inc., Madison, Wisconsin: USA ; (b) Sheldrick, G. M., *Acta Crystallogr A.* **2008**, *64* (1), 112-122.

S10. (a) Sheldrick, G. M., University of Göttingen, Germany, **2018**; (b) Sheldrick, G. M., *Acta Crystallogr. Sect. C Struct. Chem.* **2015**, *71* (1), 3-8.

S11. Hübschle, C. B.; Sheldrick, G. M.; Dittrich, B. J., *J. Appl. Crystallogr.* **2011**, *44* (6), 1281-1284.

S12. Krause, L., Herbst-Irmer, R., Sheldrick, G.M., Stalke, D., *J. Appl. Crystallogr.* **2015**, *48*, 3–10.